An Overall Study of the Asymmetrical Half-Bridge with Unbalanced Transformer Turns under Current Mode Control

Wilson Eberle, Yongtao Han, Yan-Fei Liu and Sheng Ye

Queen's Power Group
Queen's University at Kingston
Department of Electrical and Computer Engineering
Kingston Ontario Canada, K7L 3N6
wilsoneberle@wilsoneberle.com

Abstract— **An overall study of the Asymmetrical Half-Bridge (AHB) with unbalanced transformer turns under current mode control is presented. An analysis is presented for the output filter, switch stress, and dynamics. In addition, key ideas of the AHB transformer design are presented. This is followed by a survey of the existing methods that the AHB uses to achieve zero voltage switching at turn-on, namely the series inductance method and the parallel inductance method. Following these, the auxiliary L-C-C circuit method is proposed for the AHB to further minimize switching loss. Experimental results are included for a 48V/5V prototype operating at 6A load and 400kHz.**

Keywords - asymmetrical half-bridge, AHB, soft-switching, zero voltage switching, ZVS, current mode control, unbalanced turns, complementary control.

I. INTRODUCTION

The Asymmetrical Half-Bridge (AHB), illustrated in Figure 1, has been demonstrated as a good topology candidate to achieve high efficiency and good dynamic performance for low and medium power (<500W) DC-DC applications [1]-[10]. The advantages of the topology are: 1) low conduction losses in the primary switches since the voltage stress is clamped to the input, 2) Zero Voltage Switching (ZVS) can be attained for *Q1* and *Q2* at turn-on since the reflected load current is bi-directional, and 3) a small output filter can be used due to the center-tapped transformer full wave rectifier at the output.
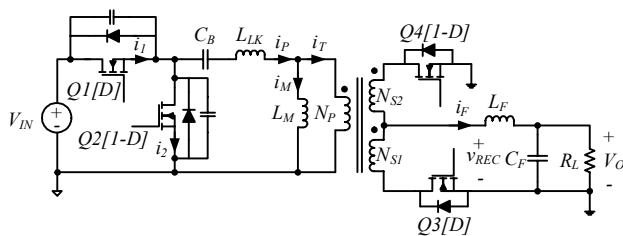
Figure 1   Asymmetrical half-bridge topology including transformer and primary switch parasitics

In addition to the advantages mentioned above, the transformer secondary turns can be unbalanced to further minimize the output filter size. Unfortunately, in all of the literature [1]-[10], except for [2],[6],[7],[9] and [10] the analysis was carried out with balanced secondary turns, $N_{S1}=N_{S2}$. Furthermore, only in [6] is any consideration given to the effects of using unbalanced turns aside from an arbitrary mathematical derivation where $N_{S1} \neq N_{S2}$. However,

the work presented in [6] only discusses the effect of unbalanced turns on the small signal dynamics under voltage mode control. Under peak current mode control, the dynamic behaviour differs significantly.

The advantages of peak current mode control are well documented: simpler dynamics, automatic over-current protection, improved line regulation, simplified current sharing and inherent avoidance of transformer saturation. For these reasons, most commercial PWM control ICs use current mode control and not voltage mode control. Dynamic analysis of the AHB has been presented in [2],[4] and [6]. However, in [2] and [4] the analysis is only presented for voltage mode control. In [6], the emphasis is voltage mode control, however one short section is included documenting the dynamic properties of the AHB with balanced transformer turns under current mode control. Unfortunately, results are not presented for unbalanced transformer turns under current mode control. Furthermore, the results presented are not necessarily optimal for current mode control since the resonant double-pole double-zero combination occurs very close to the output filter pole. Therefore, a study of the dynamics of the AHB with unbalanced turns under current mode control is necessary. In fact, it is worthwhile to study the overall steady-state, stress analysis and dynamic behaviour of the unbalanced AHB under current mode control. A detailed analysis of these concepts is presented in section II.

The main disadvantage of the AHB is the presence of a non-zero DC magnetizing current. If this non-zero DC magnetizing current is not taken into consideration in the transformer design, the transformer can easily enter saturation leading to improper operation, or even damage to the converter. The presence of this non-zero magnetizing current has been mentioned in [1],[3],[4],[7] and [9], however none of these papers discuss the impact of the DC magnetizing current on the transformer design. Since the transformer is critical to the ultimate performance and size of the converter, it is important to study the impact of the DC magnetizing current. Therefore, in section III, an overview of the key transformer design issues is presented.

As mentioned in the first paragraph, the AHB can achieve ZVS at turn-on for the primary switches because the primary current is bi-directional. Traditionally, this is accomplished using a small inductance in series with the transformer primary. This inductance includes the transformer leakage inductance and can include a small

additional series inductance. This approach has been well documented in [1],[3],[5],[7],[8] and [10]. In [9], the magnetizing inductance is used to achieve ZVS. There are advantages and disadvantages to each of these methods. Therefore, in section IV, a brief discussion of these methods is presented and an alternate auxiliary circuit method is proposed based on the L-C-C auxiliary circuit proposed in [11] and [12].

In section V, experimental results are presented for a 48V/5V unbalanced AHB operating at 6A full load and 400kHz. The conclusions are presented in section VI.

II. UNBALANCED TURNS ANALYSIS

This section includes a detailed overview of the effects of unbalanced turns on the converter output filter, switch stress and dynamics.

A. Output Filter Analysis

As mentioned in section I, one of the advantages of the AHB is the small output filter requirement due to the center-tapped full-wave rectifier. The rectified voltage waveform, v_{REC}, is given in Figure 2.
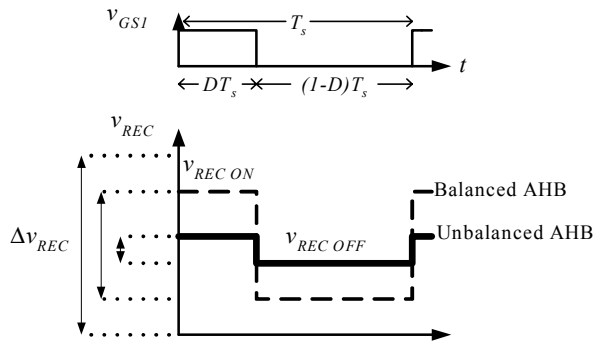
Figure 2 Secondary side rectified voltage waveform with balanced and unbalanced secondary turns

For the case with balanced transformer turns, $N_{S1}=N_{S2}=N_S$. However, if unbalanced turns are used, the turns for N_{S1} are selected as $N_{S1}<N_S$ and the turns for N_{S2} are selected as $N_{S2}>N_S$ to reduce the rectified voltage ripple, Δv_{REC} given by (1). Therefore, using unbalanced transformer turns, a further benefit can be achieved using this topology – namely a small output inductor (given by (2) for a given output filter capacitance, C_F, and output ripple requirement, Δv_O) can be used, thereby improving the load transient response characteristic.

$$\Delta v_{REC} = \frac{N_{S1}}{N_P}(1-D)V_{IN} - \frac{N_{S2}}{N_P}DV_{IN} \qquad (1)$$

$$L_F \geq \left[\frac{N_{S1}}{N_P}(1-D)V_{IN} - V_O\right]\frac{(DT_S)^2}{C_F\Delta v_O} \qquad (2)$$

B. Stress Analysis

In the steady-state, the duty ratio, D, of the AHB is given by (3) under the assumption that all switches behave ideally and that all conduction losses can be neglected. It is clear that for a given required operating point, D remains constant whether, or not N_{S1} and N_{S2} are chosen to be balanced (equal), or unbalanced (not equal).

$$D = \frac{1}{2} - \frac{1}{2}\sqrt{1 - 4\frac{V_O}{V_{IN}}\frac{1}{\left[\frac{N_{S1}}{N_P} + \frac{N_{S2}}{N_P}\right]}} \qquad (3)$$

The RMS current stress and peak voltage stress expressions are given in Table 1 for the two primary switches and two secondary rectifiers. It is clear from the expressions that since D remains fixed and the total turns ratio must remain fixed, that using unbalanced turns, $N_{S1}{\neq}N_{S2}$, does not affect the switch stress, or more importantly, the steady-state power sharing between the switches.

TABLE I. CURRENT AND VOLTAGE STRESSES FOR THE PRIMARY SWITCHES AND RECTIFIERS OF THE AHB

	RMS Current Stress	
Q_1	$\sqrt{D}\sqrt{\left(\left[\frac{N_{S1}}{N_P} + \frac{N_{S2}}{N_P}\right](1-D)I_O\right)^2 + \frac{\Delta i_{Q1}^2}{12}}$	(4)
Q_2	$\sqrt{1-D}\sqrt{\left(\left[\frac{N_{S1}}{N_P} + \frac{N_{S2}}{N_P}\right]DI_O\right)^2 + \frac{\Delta i_{Q2}^2}{12}}$	(5)
Q_3	$\sqrt{D}\sqrt{I_O + \frac{\Delta i_F^2}{12}}$	(6)
Q_4	$\sqrt{1-D}\sqrt{I_O + \frac{\Delta i_F^2}{12}}$	(7)
	Peak Voltage Stress	
Q_1	V_{IN}	(8)
Q_2	V_{IN}	(9)
Q_3	$\left[\frac{N_{S1}}{N_P} + \frac{N_{S2}}{N_P}\right]DV_{IN}$	(10)
Q_4	$\left[\frac{N_{S1}}{N_P} + \frac{N_{S2}}{N_P}\right]DV_{IN}$	(11)

C. Dynamic Analysis

The AHB powertrain is relatively complicated. It is a fourth-order system due to the four energy storage elements, L_M, C_B, L_F and C_F. Under voltage mode control, the control-to-output transfer function exhibits four-poles and two-zeroes. The four-poles occur as a pair of double-poles and the two-zeroes occur together as a double-zero [4]. The output filter double-pole can be approximated by (12) and the L_MC_B double-pole can be approximated by (13). The double-zero location can be approximated by (14).

$$f_{FDP} \approx \frac{1}{2\pi\sqrt{L_FC_F}} \qquad (12)$$

$$f_{BDP} \approx \frac{1}{2\pi\sqrt{L_M C_B}} \qquad (13)$$

$$f_{BDZ} \approx \frac{\sqrt{K}}{2\pi\sqrt{L_M C_B}} \qquad (14)$$

The K term in (14) is related to the transformer turns and steady-state duty cycle. It is always greater than one. Therefore the $L_M C_B$ double-zero always occurs after the $L_M C_B$ double-pole. Furthermore, with unbalanced turns, K increases, so the double-zero moves further away from the double-pole.

The AHB large signal model presented in [10] can be used to predict the converter small signal behaviour and transfer functions under current mode control, so that the converter poles and zeroes can be determined using SPICE for a given operating point. Unfortunately, deriving closed-form expressions for the exact pole-zero locations under current mode control is very difficult. However, the voltage mode control explanation can be extended qualitatively to current mode control. Under current mode control, the output filter double-pole separates into two poles. The capacitor pole moves to a lower frequency and the inductor pole moves to a higher frequency approaching the switching frequency. Therefore, the system effectively becomes a three-pole two-zero system. The dominant low frequency pole is due to the output filter capacitor and the load. The second double-pole can still be approximated by (13) and the double zero can be approximated by (14).

This behaviour can best be demonstrated with an example using the model presented in [10] with the following parameters: V_{IN}=48V, V_O=5V, I_{Load}=6A, F_S=400kHz, C_F=50µF, C_B=2.2µH, L_M=25µH and N_P=6. Since a smaller output filter inductor can be used with unbalanced turns to achieve similar filter inductor ripple current, L_F was selected as 1µH for the unbalanced AHB and 4.7µH for the balanced AHB. For the unbalanced AHB the secondary turns were selected as N_{S1}=1 and N_{S2}=3. Therefore, for the balanced AHB, N_S=2.

The control-to-output magnitude and phase responses are plotted in Figure 3 for the AHB with balanced turns and unbalanced turns. It is noted that with unbalanced turns, the double-pole double-zero combination spreads out as predicted by the voltage mode control model. In addition, with balanced turns, the double-pole occurs earlier since a larger filter inductor must be used. This behaviour is not immediately clear from (13), however it is noted that the four-poles are actually coupled, so (12)-(14) are only approximations. If L_M in (13) is replaced by L_{eq} which is a function of L_M and L_F, and if L_F is increased with balanced turns, then L_{eq} increases. Therefore, as L_{eq} increases, the pole location given by (13) decreases, which explains the leftward shift of the double-pole in Figure 3 occurring at approximately 20kHz for the AHB with balanced turns. The double-pole of the AHB with unbalanced turns occurs at approximately 50kHz.

It is clear from the behaviour that superior dynamic response can be achieved with unbalanced turns since the resonant double-pole of the converter occurs at a higher frequency allowing the use of a wider band feedback loop.
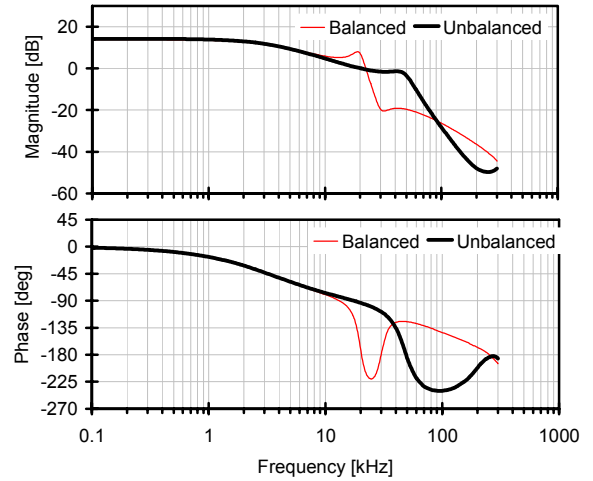
Figure 3   Comparison of the balanced and unbalanced AHB control-to-output magnitude (top) and phase (bottom) responses at 5V/6A load, 48V input and 400kHz switching frequency

III. TRANSFORMER DESIGN CONSIDERATIONS

As mentioned in the introduction, the AHB operates with a DC bias current, I_M, through the magnetizing inductance, as given by (15). This current is due to the imbalance in the reflected load current, which cannot pass through the blocking capacitance.

$$I_M = \frac{N_{S2}}{N_P}(1-D)I_O - \frac{N_{S1}}{N_P}DI_O \qquad (15)$$

This DC component increases with increasing load current and increasing input voltage (since D decreases as V_{IN} increases). In addition, it increases with unbalanced turns since the ratio N_{S2}/N_P increases and the ratio N_{S1}/N_P decreases. Unfortunately, this DC current can easily saturate the transformer if it is ignored during the design process. The saturation can be explained using the B-H curve illustrated in Figure 4. Since the magnetic field is proportional to current, it is clear that if the core is ungapped then the DC magnetizing current, I_M, will easily saturate the core. In order to avoid saturation, the core can be gapped, which skews the B-H curve of the core to the right in the first quadrant. If sufficient gap is added to the core, the core can avoid saturation and operate in the shaded region in the first quadrant of the B-H curve.

As indicated in the Figure, gapping the core decreases the permeability of the core, μ, which has the effect of decreasing the magnetizing inductance, L_M. This agrees with the traditional method of calculating an inductance with a gapped core as given by (16), where l_g is the gap length and A_E is the effective cross sectional area of the core.
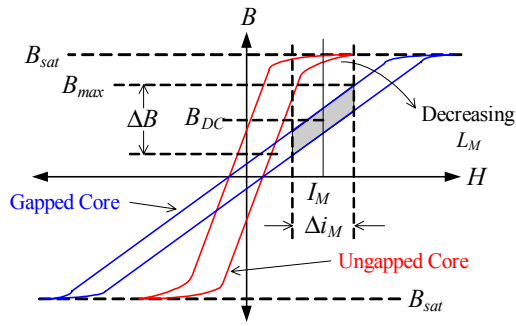
Figure 4   Comparison of the B-H curves for gapped and ungapped cores operating with a DC magnetizing current I_M

$$L_M = \frac{\mu_O A_E N_P^2}{l_g} \qquad (16)$$

However, it is worth noting that it is not always practical, or desired to decrease L_M too much by increasing the air gap length in order to avoid saturation. If a specific value of L_M is desired, the core size can be increased by increasing A_E in (16) to achieve the desired L_M.

Equation (16) neglects the fringing effects at the gap and the permeability of the core. More accurate estimates of the required gap length and magnetizing inductance can be calculated using (17) and (18) respectively.

$$l_g = \frac{N_P I_M + \frac{D(1-D)V_{IN}Ts}{2N_P A_L} - B_{\max}\frac{l_e}{\mu_0\mu_r}}{\frac{B_{\max}}{\mu_0\eta} - B_{\max}\frac{1}{\mu_0\mu_r} - \frac{D(1-D)V_{IN}Ts}{2N_P A_L l_e}\left(\frac{\mu_r}{\eta}-1\right)} \qquad (17)$$

$$L_M = \frac{A_L N_P^2}{\left[\frac{\mu_r}{\eta}-1\right]\frac{l_g}{l_e}+1} \qquad (18)$$

The parameters in (17) and (18) are as follows:
μ_O: permeability of free space
μ_r: relative permeability of the material
l_e: effective magnetic path length of the core
η: a correction factor between 1.05 and 1.1 for the cross-sectional area of the core due to the fringing effect
A_L: inductance factor provided by the manufacturer without the air gap
$B_{\max}$: maximum operating flux density selected for the design

IV. SOFT-SWITCHING ANALYSIS

It was mentioned in section I that the AHB can achieve ZVS at turn-on for the two primary switches. Qualitatively, this is clear since the primary current, i_P, is bi-directional and the leakage inductance (and any additional series inductance) at the transformer primary will always tend to discharge the output capacitance of the switch that is about to turn-on during the dead-time between the switching transition. This is the traditional method used to achieve ZVS at turn-on for the primary switches. The primary side current waveforms are given in Figure 5 to illustrate this

concept. In order to achieve ZVS at turn-on for $Q1$, the primary current i_P at time t_b should be negative so that during the dead time between the turn-off of $Q2$ and turn on of $Q1$, the output capacitance, $C2$, of $Q2$ is charged and the output capacitance, $C1$, of $Q1$ is discharged. Conversely, in order to achieve ZVS at turn-on for $Q2$, the primary current i_P at time t_a should be positive so that during the dead time between the turn-off of $Q1$ and turn on of $Q2$, the output capacitance, $C1$, of $Q1$ is charged and the output capacitance, $C2$, of $Q2$ is discharged.

The ability to achieve ZVS using this method for each switch depends greatly on the load current and leakage inductance. Therefore it is useful to express the necessary conditions to achieve ZVS in terms of the energy in the parasitic elements. Expressions can be derived for the required load current and/or leakage inductance to achieve ZVS for each switch. The required leakage inductance to achieve ZVS for $Q1$ is given by (19) and the required leakage inductance to achieve ZVS for $Q2$ is given by (20). These relationships assume that the output filter inductor current ripple is negligible ($i_F=I_O$) and that the transformer magnetizing current ripple is negligible ($i_M=I_M$). It is clear from these equations that as the load current increases, the required leakage, or series inductance decreases. Furthermore, these relationships are useful since the transformer primary leakage inductance is the most difficult parameter to measure accurately. The other parameters can be measured, or obtained from data sheets. It is noted that using unbalanced transformer turns does not affect the converters ability to achieve ZVS for either switch.

$$L_{LK} \geq \frac{(C1+C2)}{I_O}\frac{1}{\left[\frac{N_{S1}}{N_P}+\frac{N_{S2}}{N_P}\right]^2}\left(\frac{V_{IN\max}}{D_{\min}}\right)^2 \qquad (19)$$

$$L_{LK} \geq \frac{(C1+C2)}{I_O}\frac{1}{\left[\frac{N_{S1}}{N_P}+\frac{N_{S2}}{N_P}\right]^2}\left(\frac{V_{IN\max}}{(1-D_{\min})}\right)^2 \qquad (20)$$

The advantage of this method is that no additional components are needed – the converter can achieve ZVS using the energy in its own parasitic elements. In addition, ZVS is achieved easier as load increases. Therefore, switching losses are reduced or eliminated as conduction losses increase with load.

The disadvantages of this method are: 1) loss of ZVS at light load, 2) duty cycle loss if large L_{LK} is required and 3) ringing on the output rectifiers. Furthermore, it is more difficult to achieve ZVS for $Q1$ than $Q2$ since the DC value of the $Q2$ current is less than $Q1$. This can also be observed by inspection of (19) and (20) since a larger leakage inductance is required for $Q1$ because $D_{\min}<(1-D_{\min})$.

The other common method proposed to achieve ZVS utilizes the transformer magnetizing inductance. In this method, the transformer is designed with a small magnetizing inductance so that the transformer magnetizing current contains a large ripple component. This is illustrated

in Figure 5 by the dotted waveforms, i_M', i_P', i_1' and i_2'. Therefore, $Q1$ can achieve ZVS easier at turn-on since the primary current at the beginning of the instant, t_b is large negative. Similarly, $Q2$ can achieve ZVS easier at turn-on since the primary current at the beginning of the instant, t_a is large positive.
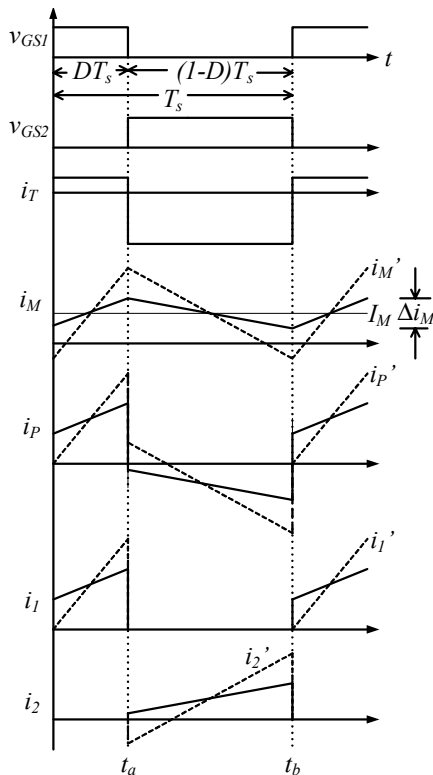
Figure 5   Primary current waveforms for the AHB

If this method is used to achieve ZVS turn-on of the primary switches, the maximum magnetizing inductance that can be used is given by (21).

$$L_M \leq \frac{V_O}{2 f_S \left[\dfrac{N_{S1}}{N_P} + \dfrac{N_{S2}}{N_P} \right]^2 I_O (1 - D_{\min})} \tag{21}$$

If this method is used, the transformer can be designed with minimal leakage inductance, so that duty cycle loss and ringing on the output rectifiers are minimized. In addition, no additional components are needed to achieve ZVS - the small leakage inductance can be achieved by increasing the gap in the transformer core, which is not a problem since the AHB transformer typically requires a gap to avoid saturation as discussed in section III.

There are several disadvantages to this method: 1) primary side conduction losses increase due to the higher peak currents, and 2) this method is not well suited to low output voltage, high load current applications since the magnetizing inductance must be made very small.

The AHB with an auxiliary L_a-C_{a1}-C_{a2} circuit is proposed in Figure 6. This circuit has been successfully implemented with the phase shift full-bridge and the asymmetrical PWM resonant converter in previous literature. The auxiliary circuit can help switches $Q1$ and $Q2$ achieve ZVS at turn-on by the injection of an AC triangular ripple current into the node connecting the two switches.
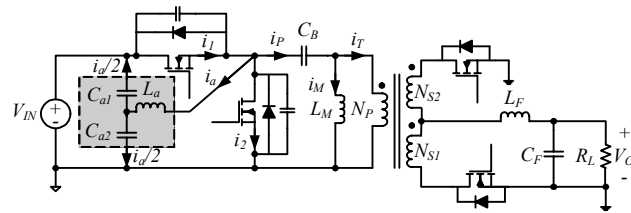
Figure 6   Asymmetrical half-bridge with auxiliary L-C-C circuit
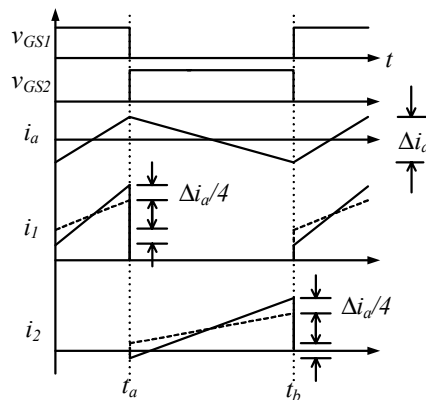
Figure 7   Waveforms of the AHB with auxiliary L-C-C cirucit

The waveforms for the auxiliary circuit are illustrated in Figure 7. Capacitors C_{a1} and C_{a2} are large so the voltage across each of them can be considered constant. The average voltage across the inductor must be zero, therefore the voltage across C_{a2} is DV_{IN}. The node connecting the source of $Q1$ and the drain of $Q2$ alternates polarity between V_{IN} and ground. When Q_1 conducts, the voltage across the inductor is $(1-D)V_{IN}$, so the inductor current ramps up in the positive direction indicated by i_a. When $Q2$ conducts, the voltage across the inductor is $-DV_{IN}$, so the inductor current ramps down. The total auxiliary current splits between the two capacitors, so the additional ramp current injected into each switch is $2(\Delta i_a/4) = \Delta i_a/2$ as indicated in Figure 7 by the solid lines. This ripple current helps each switch achieve ZVS at turn-on in a similar manner to the approach using the magnetizing inductance. At time t_a, when $Q2$ is about to turn-on, i_a is instantaneously positive, so it helps discharge the output capacitance of $Q2$ during the dead time between the switching transition. At time t_b, when $Q1$ is about to turn-on, i_a is instantaneously negative, so it helps charge the output capacitance of $Q2$ and discharge the output capacitance of $Q1$ during the dead time.

The main advantage to this approach is that ZVS turn-on can be achieved independent of the line voltage, or load current. In addition, if sufficient energy is injected using the auxiliary circuit approach, snubber capacitors can be placed across $Q1$ and $Q2$ to reduce turn-off loss. It is also noted that the additional ramp current only conducts through the switches and not the transformer windings.

V. EXPERIMENTAL RESULTS

A 30W, 5V output prototype of the AHB was built on a ten-layer printed circuit board with 1.5 ounce copper as shown in Figure 8. The input voltage range was 35-75V. The switching frequency was 400kHz. The transformer turns were selected as follows: N_P=6, N_{S1}=1 and N_{S2}=3. The steady-state, dynamic and efficiency results are given in this section.

Figure 8   48V/5V, 30W, 400kHz AHB prototype

It was discussed in section IV that the primary switches of the AHB can achieve ZVS at turn-on. This is demonstrated in Figure 9. It is clear that switch $Q2$ turns on with ZVS since the drain voltage, v_{DSQ2}, reaches zero volts before the gate voltage, v_{GSQ2} turns-on.

The rectified voltage waveform, v_{REC}, and output voltage waveform, V_O, are shown in Figure 10. It is clear that using unbalanced turns can minimize the size of the output filter. The rectified voltage ripple (ignoring the commutation intervals) in Figure 10, is only 1V.
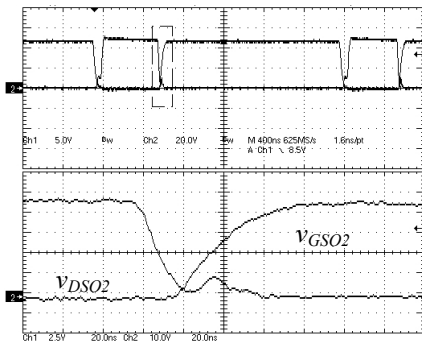
Figure 9   Q2 drain-to-source and gate-to-source waveforms; soft-switching is achieved
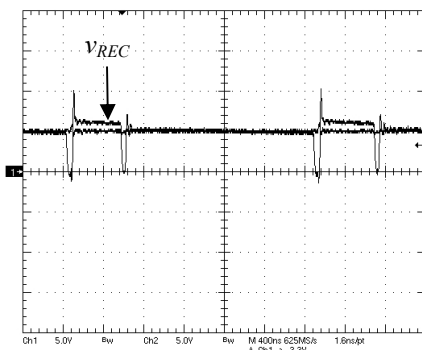
Figure 10   Secondary rectified voltage, v_{REC}, waveform and output voltage, V_O

The converter control-to-output response (Figure 11) and loop response (Figure 12) were measured and compared to the responses predicted by the dynamic model proposed in [10]. A loop bandwidth of 13kHz was achieved at a phase margin of 48 degrees and a gain margin of 10dB.
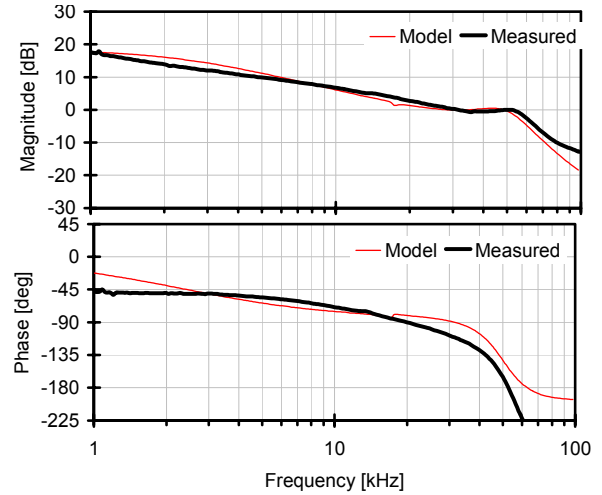
Figure 11   Unbalanced AHB control-to-output magnitude (top) and phase (bottom) responses
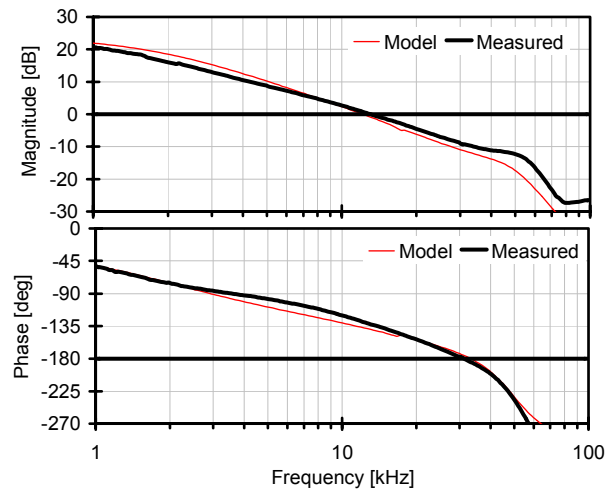
Figure 12   Unbalanced AHB loop magnitude (top) and phase (bottom) responses

The efficiency of the prototype was measured as a function of load current and input voltage as shown in Figure 13 and Figure 14 respectively. A peak efficiency of 89.8% was achieved at 4.5A load. The auxiliary L-C-C circuit was not used in the experiments in order to keep the size of the prototype minimized. However, it is the opinion of the authors that the efficiency of the converter could be improved at light load and maximum input by using the auxiliary circuit. Further improvement would also be expected if thicker PCB copper traces were used.
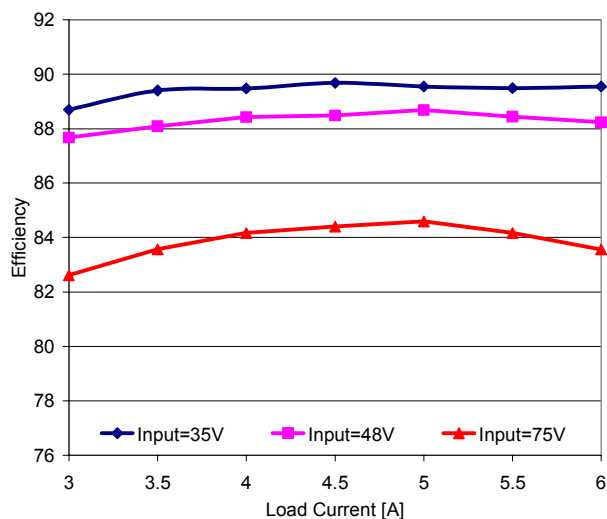
Figure 13   Unbalanced AHB efficiency as a function of load at 5V output and 400kHz switching frequency
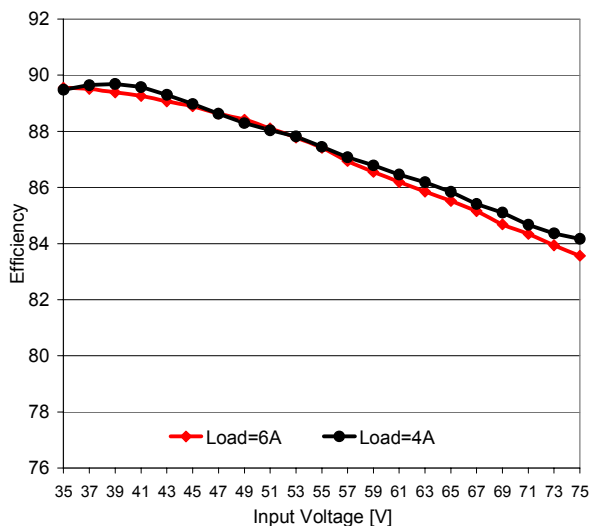
Figure 14   Unbalanced AHB efficiency as a function of input voltage at 5V output and 400kHz switching frequency

VI. CONCLUSIONS

An overall study of the asymmetrical half-bridge with unbalanced transformer turns under current mode control was presented. An analysis was presented for the output filter, switch stress and dynamic analysis. Using unbalanced transformer secondary turns can reduce the output filter size, thereby improving transient response. There is no effect on the switch stress using unbalanced transformer turns. Dynamic analysis illustrates that peak current mode control splits up the double-pole due to the output filter capacitance and output filter inductance. With unbalanced turns, the double-zero due to the blocking capacitance and magnetizing inductance moves to a frequency beyond the converter's crossover frequency. Greater loop bandwidth can be achieved with unbalanced turns.

The DC component of the magnetizing current must be considered in the transformer design. Designing the transformer usually requires a compromise between the core

size and air gap length. Increasing the air gap helps avoid saturation, however the magnetizing inductance decreases. Increasing the core size increases the magnetizing inductance.

The AHB can achieve ZVS at turn-on for the primary switches. The traditional methods include using 1) a series inductance with the transformer primary, which can consist of the leakage inductance, and 2) parallel inductance consisting of the transformer magnetizing inductance. These methods are not optimal for all line and load conditions, so an auxiliary L-C-C circuit can be used to further reduce switching loss.

A prototype of the AHB with unbalanced transformer turns was built. Steady-state, dynamic and efficiency results were presented for the converter operating with a 35-75V input range and a 5V, 30W load at 400kHz. In all cases the results agree with the predicted theory.

REFERENCES

[1] P. Imbertson and N. Mohan, "Asymmetrical Duty Cycle Permits Zero Switching Loss in PWM Circuits with No conduction Loss Penalty," IEEE Transactions on Industry Applications, Vol. 29, No. 1, January/February 1993, pp. 121-125.

[2] S. Korotkov, V. Meleshin, A. Nemchinov and S. Fraidlin, "Small-Signal Modeling Of Soft-Switched Asymmetrical Half-Bridge DC/DC Converter," IEEE Applied Power Electronics Conference (APEC), 1995, pp. 707-711.

[3] O. Garcia, J.A. Cobos, J. Uceda and J. Sebastian, "Zero Voltage Switching in the PWM Half Bridge Topology with Complementary Control and Synchronous Rectification," IEEE Power Electronics Specialists Conference (PESC), 1995, pp. 286-291.

[4] J. Sebastian, J.A. Cobos, O. Garcia and J. Uceda, "An Overall Study of the Half-Bridge Complementary-Control DC-to-DC Converter," IEEE Power Electronics Specialists Conference (PESC), 1995, pp. 1229-1235.

[5] L. Xiao and R. Oruganti, "Soft Switched PWM DC/DC Converter With Synchronous Rectifiers," IEEE International Telecommunications Energy Conference (INTELEC), 1996, pp. 476-484.

[6] F. Linera, J. Sebastian, M.A. Perez Garcia, J. Diaz and A. Fontan, "Closing the Feedback Loop in the Half-Bridge Complementary-Control DC-to-DC Converter," IEEE Applied Power Electronics Conference (APEC), 1997, pp. 977-982.

[7] S. Korotkov, V. Meleshin, R. Miftahutdinov and S. Fraidlin, "Soft-Switched Asymmetrical Half-Bridge DC/DC Converter: Steady-State Analysis. An Analysis Of Switching Processes," Telecommunications and Energy Specialists Conference (TELESCON), 1997, pp. 177-184.

[8] R. Oruganti, P.C. Heng, J.T.K. Guan and L.A. Choy, "Soft-Switched DC/DC Converter with PWM Control," IEEE Transactions on Power Electronics, Vol. 13, No. 1, January 1998, pp. 102-114.

[9] J. Feng, Y. Hu, W. Chen and C. Wen, "ZVS Analysis of Asymmetrical Half-Bridge Converter," IEEE Power Electronics Specialists Conference (PESC), 2001, pp. 243-247.

[10] W. Eberle and Y.F. Liu, "A Zero Voltage Switching Asymmetrical Half-Bridge DC/DC Converter With Unbalanced Secondary Windings for Improved Bandwidth," IEEE Power Electronics Specialists Conference (PESC), 2002, Vol. 4, pp. 1829-1834.

[11] P. Jain, W. Kang, H. Soin and Y. Xi, "Load and Line Independent Zero Voltage Switching DC/DC Converter Topology," IEEE International Telecommunications Energy Conference (INTELEC), 1998, pp. 22-29.

[12] S. Mangat, Y. Xi, P. Jain and Y.-F. Liu, "A Modified Asymmetrical Pulse-Width-Modulated Resonant DC/DC Converter Topology," IEEE Power Electronics Specialists Conference (PESC), 1998, pp. 662-668.